Investigation of Thermally Responsive Block Copolymer Thin Film Morphologies Using Gradients

Jennifer Y. Kelly,[†] Julie N. L. Albert,[‡] John A. Howarter,[†] Shuhui Kang,[†] Christopher M. Stafford,[†] Thomas H. Epps III,*[,‡] and Michael J. Fasolka*[,†]

Polymers Division, National Institute of Standards and Technology, Gaithersburg, Maryland 20899, United States, and Department of Chemical Engineering, University of Delaware, Newark, Delaware 19716, United States

ABSTRACT We report the use of a gradient library approach to characterize the structure and behavior of thin films of a thermally responsive block copolymer (BCP), poly(styrene-*b*-*tert*-butyl acrylate) (PS-*b*-P*t*BA), which exhibits chemical deprotection and morphological changes above a thermal threshold. Continuous gradients in temperature and film thickness, as well as discrete substrate chemistry conditions, were used to examine trends in deprotection, nanoscale morphology, and chemical structure. Thermal gradient annealing permitted the extraction of transformation rate constants (k_t) for the completion of thermal deprotection and rearrangement of the film morphology from a single BCP library on hydroxyl and alkyl surfaces, respectively. The transformation rate constants ranged from 1.45×10^{-4} s^{-1} to 5.02×10^{-5} s^{-1} for temperatures between 185 and 140 °C for hydroxyl surfaces. For the same temperature range, the alkyl surfaces yielded k_t values ranging from 4.76×10^{-5} s^{-1} to 5.73×10^{-6} s^{-1}, an order of magnitude slower compared to hydroxyl surfaces. Activation energies of the thermal deprotection and film transformation on these surfaces were also extrapolated from linear fits to Arrhenius behavior. Moreover, we noted a morphology shift and orientation transformation from parallel lamellae to perpendicular cylinders at the free surface because of changes in volume fraction and surface energetics of the initially symmetric BCP. Using gradient techniques, we are able to correlate morphological and chemical structure changes in a rapid fashion, determine kinetics of transitions, and demonstrate the effect of surface chemistry on the deprotection reaction in thermally responsive BCP thin films.

KEYWORDS: block copolymer • thermal deprotection • surface energetics • surface chemistry • gradient • morphology • thin film • film thickness

INTRODUCTION

Block copolymer (BCP) self-assembly is widely recognized for its potential in nanofabrication (1−4), and many examples in the literature demonstrate how these materials can be harnessed for a wide variety of technologies including smart coatings (5), (bio)sensors (6), molecular transfer printing (7), advanced separations (8), antifouling and antibacterial coatings (8), and flexible electronics (9, 10), as well as for mimicking biological interfaces (8, 10−12). BCP self-assembly in thin films is a complex phenomenon, with a large parameter space, including film thickness, temperature, molecular mass, and surface energy, governing the film morphology (10, 13−22). This complexity is compounded when considering the behavior of functional, thermally responsive BCP thin films.

The thermocleavable behavior of the poly(*tert*-butyl acrylate) (P*t*BA) block in poly(styrene-*b*-*tert*-butyl acrylate) (PS-*b*-P*t*BA) BCPs is a prime example of such complexity (see Scheme 1). The effect of interfacial confinement on the deprotection kinetics of this thermally responsive BCP system has been studied previously (11). Composto and co-workers examined the ordering and stimuli-responsive reversibility of the BCP deprotection in an asymmetric PS-*b*-P*t*BA copolymer (6, 23, 24). These researchers showed how a cylinder-forming amphiphilic BCP created ordered nanostructures that could be employed as nanoscale templates for organizing biopolymers and pH-responsive devices. In their work, the asymmetric BCP thin film was annealed at 130 °C for 2 days, and the *tert*-butyl group was cleaved, leading to the formation of a carboxylic acid group. Nealey and co-workers utilized a similar asymmetric PS-*b*-P*t*BA BCP to fabricate linear arrays of nanodots of spherical domains for ordered geometries of nanoparticles (25, 26). The nanodot arrays were produced through a thermochemically induced cylinder-to-sphere morphological transition accomplished by annealing a thin film of the asymmetrical PS-*b*-P*t*BA BCP at 160 °C for 24 h. Thermal deprotection resulted in the formation of a poly(acrylic anhydride) (PAH) BCP, the dehydrated analogue of poly(acrylic acid) (PAA) (26). Annealing the same film at 130 °C for 2 days, however, did not give the deprotected BCP in the study by Nealey and co-workers (26). The discrepancies in the thermal behavior reported by Composto et al. and Nealey et al. highlight the need to further examine the behavior of this system, as well as the need for methods that can map such behavior in a comprehensive and rapid manner.

* To whom correspondence should be addressed. E-mail: thepps@udel.edu (T.H.E.); michael.fasolka@nist.gov (M.J.F.).
Received for review August 05, 2010 and accepted October 04, 2010
[†] National Institute of Standards and Technology.
[‡] University of Delaware.
DOI: 10.1021/am100695m

Scheme 1. Proposed Chemical Transformation of PS-*b*-P*t*BA to PS-*b*-PAH (and PS-*b*-PAA) via Thermal Deprotection of the *tert*-Butyl Acrylate Linkage

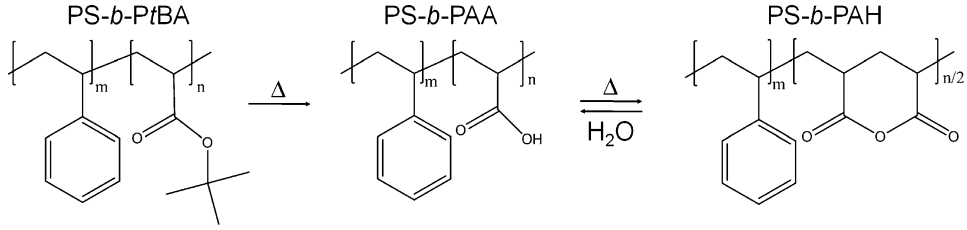

To this end, we applied gradient library approaches to probe the parameters that affect deprotection and morphological trends in thin films of this block copolymer. Gradient techniques enable the rapid and systematic analysis of key factors as well as the mapping of wide ranges of thin film behavior using a single specimen and a single processing step. The use of gradients has facilitated the study of film thickness, temperature, and surface energy effects on the self-assembly of "simple" di- and triblock copolymers (13, 20, 22, 27, 28), but has not yet been extended to examine more complex systems such as the thermally responsive materials studied in this work. The use of gradients herein enables the rapid investigation of morphology and chemical structure of a volume-symmetric PS-*b*-P*t*BA BCP as a function of temperature, film thickness, and substrate surface chemistry. As such, thermal and thickness gradients were utilized to probe a continuous series of annealing temperatures and thicknesses, which enabled quantification of the deprotection reactions (and their effects on BCP morphology). The use of thermal and thickness gradients has been proven to be especially valuable in examining and mapping phenomenon such as polymer dewetting (29), phase separation in polymer blends (30), and thin film crystallization behavior (31, 32). Herein, kinetic parameters were extracted from single-gradient library measurements, an approach that can mitigate experimental uncertainties arising from multiple discrete experiments.

EXPERIMENTAL SECTION

General. Certain commercial materials and equipment are identified in this paper to specify experimental procedures. In no case does such identification imply recommendation by the National Institute of Standards and Technology (NIST) nor does it imply that the materials and equipment identified are necessarily the best available for this purpose.

Materials. The PS-*b*-P*t*BA diblock copolymer examined was purchased from ATRP Solutions. The polymer number average molar mass was M_n = 11,200 g/mol (reported by ATRP Solutions, Inc.), and the volume fraction of the PS block before deprotection was calculated to be $\phi_{PS} = 0.47$. The polydispersity index was 1.14 (reported by ATRP Solutions, Inc.). More details on the BCP are given in Tables 1 and 2.

Substrate Preparation. Silicon wafers (*N* <100>, Wafer World, Inc.) were rinsed with toluene, placed in an ultraviolet-ozone (UVO) cleaner for 10 min (Model 342, Jelight Co., Inc.), then rerinsed with toluene prior to use. To create alkyl functionalized substrates, silicon wafers were rinsed with toluene and processed in a UVO cleaner, then placed in a vacuum desiccator along with a Teflon boat containing ≈0.5 mL of *n*-octyldimethylchlorosilane (ODS). A low vacuum, applied to the desiccator, helped saturate the chamber with ODS vapor, which reacted with the silanols on the substrate surface. After a saturated vapor exposure of 6 h, the substrate was removed from the desiccator, rinsed with toluene, and dried with a stream of dry nitrogen.

Film Preparation. Uniform thickness BCP films were deposited on both UVO-treated and ODS-modified silicon substrates by flow-coating (27). This method creates films by spreading a layer of polymer solution over the substrate using a knife blade. For our studies, 50 μL of a 3% by mass PS-*b*-P*t*BA polymer in toluene was spread by a blade fixed 200 μm above the substrate surface, with substrate velocities set to achieve film thicknesses (h) of ≈100 nm. Film dimensions were 10 mm by 55 mm. To create film thickness libraries, the flow coater blade was accelerated during the solution spreading process to create a thickness gradient as the solution dries (27). Using the solution concentration and blade gap described above, the acceleration was set to achieve a film thickness range from 65 to 105 nm. Film dimensions of the thickness gradient samples were 50 mm by 55 mm. Film thickness was measured using reflectance interferometry (Model F20, Filmetrics). Atomic force microscopy (AFM) scratch tests were also used to verify film thickness at specific locations.

For the films annealed on a thermal gradient (described below), specimens were first annealed under vacuum at 110 °C overnight (≈18 h) to remove any residual solvent. No thermal deprotection occurred at 110 °C, as determined by X-ray photoelectron spectroscopy. For films annealed isothermally under vacuum, specimens were placed in a vacuum oven at the designated temperature and annealed for 24 h. Upon removal from the oven, specimens were immediately quenched to room temperature on a metal plate.

Thermal Gradient Annealing. A gradient hot stage exhibiting a linear temperature gradient (≈10 °C/cm, see Figure S1) was used to study the effect of temperature on the deprotection reaction. The high-temperature end of the stage was heated using a resistive heating element regulated with a thermal controller set to 250 °C, and the low-temperature end of the

Table 1. Properties of the BCP before and after Deprotection

property	before deprotection	after deprotection
structure	PS-*b*-P*t*BA	PS-*b*-PAH
composition (ϕ_{PS})	0.47	0.62
molecular mass (g/mol)	11,200	8,200
bulk morphology	lamellae	cylinders
film thickness	h	0.7 h

Table 2. Molecular Characteristics of PS, P*t*BA, and PAH

	PS	P*t*BA	PAH
M_n (g/mol)	5200	6000	3000
ρ (g/cm^3)(35)	1.05	1.04	1.12
v (cm^3/mol)	4953	5769	2648

stage was cooled by a refrigerated recirculation bath set to 22 °C. The temperature was calibrated along the gradient using a separate thermocouple and a thermal infrared camera (FLIR Systems Thermovision A20). In the direction perpendicular to the thermal gradient, the temperature was uniform; thus each temperature across the width of the sample could be correlated to a position for comparing various characterization techniques. Library samples were placed at specific locations on the temperature stage based on the desired temperature range to be studied.

Polarization Modulation−Infrared Reflection Absorption Spectroscopy (PM-IRRAS). The PM-IRRAS measurements were performed on a Nicolet 6700 FT-IR spectrometer, equipped with an external tabletop optical mount, which included a photoelastic modulator (PEM) with a modulation frequency of 50 kHz, a synchronous sampling demodulator, and a MCT-A detector. The IR spectra were recorded with Omnic software by setting the PEM half-wave retardation at 1700 cm^{-1}. 1000 scans were added and averaged for each spectrum with a resolution of 8 cm^{-1}, and the beam incident angle was set to 70° to achieve a high signal-to-noise ratio. All IR spectra were collected at ambient conditions. Due to the phase modulation technique, no reference sample was needed in the experiments, and the random noise from moisture and CO_2 was effectively suppressed (33).

Optical and Atomic Force Microscopy. Optical microscopy images were collected on a Nikon microscope equipped with a CCD camera at 50× magnification. Tapping mode AFM images were collected using a Veeco Dimension 3100 AFM with a Nanoscope IV control unit. Silicon probes (Nanosensors) with a resonant frequency between 146 kHz and 236 kHz and a force constant between 21 N/m and 98 N/m were used to image the polymer films. Domain spacing (L_0) was measured for PS-*b*-P*t*BA based on island height measurements (14 nm) and for PS-*b*-PAH based on cylinder center-to-center measurements (13 nm) via AFM.

X-ray Photoelectron Spectroscopy (XPS). X-ray photoelectron spectroscopy (XPS) was performed on a Kratos Axis Ultra spectrometer using monochromatized Al K_α radiation at 1486.6 eV. Survey spectra were taken at 90° (normal to the specimen surface) at three unique locations for each measurement along the deprotection front and spaced in 1 mm increments across 16 mm. Each survey spectrum was a sum of five scans acquired at pass energy of 160.0 eV and resolution of 0.5 eV/step. Dwell time was 100 ms/step for survey scans. A neutralizer gun was used to reduce charging of the samples. Binding energy corrections were made by referencing spectra to the C 1s peak at 285.0 eV. Relative atomic concentrations were determined by subtracting a Shirley-type background and subsequently integrating the area under the remaining peak and dividing by the relative sensitivity. The relative sensitivity factors were provided by the manufacturer and are as follows: O 1s = 0.780, C 1s = 0.278, Si 2p = 0.328. A transmission function correction was also made. The program used for quantification was CasaXPS. The standard uncertainty associated with XPS measurement was 2%.

The chemical transition due to thermal deprotection was characterized using high-resolution spectra of the C 1s region measured at each location. Each high-resolution spectrum was acquired at pass energy of 20.0 eV and resolution of 0.1 eV/step. The high-resolution carbon spectra were modeled by assigning five peaks representing the major constituents: aromatic carbon at 284.75 eV, aliphatic carbon at 285.0 eV, *tert*-butyl carbon at 287.0 eV, carbonyl carbon at 289.5 eV, and the shakeup peak due to π-bond resonance at 291.0 eV. Peak locations and full-width half-maximum values were constrained based on standard data sets in The XPS of Polymers Database (34).

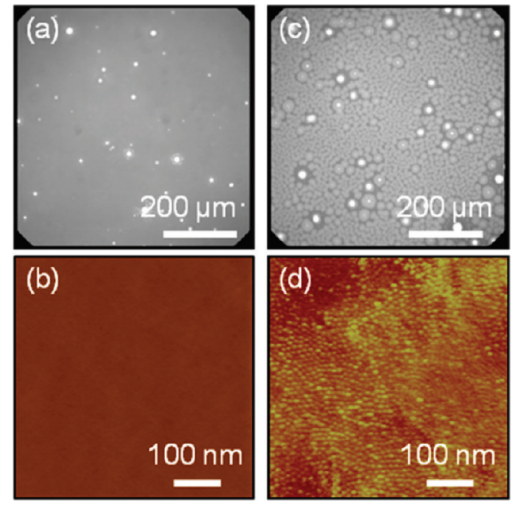

FIGURE 1. Optical and AFM images of (a, b) PS-*b*-P*t*BA and (c, d) PS-*b*-PAH on the UVO-treated of silicon. (a, c) Optical micrographs show island/hole features. (b, d) AFM phase images suggest (b) parallel lamellar structures and (d) perpendicular cylindrical structures. Images a and b were taken after annealing for 24 h at 130 °C where no deprotection occurs, whereas images c and d were taken after annealing for 24 h at 150 °C where deprotection occurs. The *z*-scale for both AFM phase images is 10°.

RESULTS AND DISCUSSION

To validate the gradient methodology, thermal behavior, and self-assembly of PS-*b*-P*t*BA thin films, uniform specimens were examined before and after isothermal annealing at several temperatures. Subsequently, gradients in temperature and film thickness were used to examine the system in a more comprehensive manner. Substrate surface chemistry was also varied to investigate the effects of a hydroxyl versus an alkyl substrate surface. These parts of the study will be discussed in turn.

Isothermal Annealing. Isothermal annealing studies enabled examination of the basic thermal behavior of the block copolymer films, which are summarized in Table 1. Annealing the films under vacuum, or in air, for 24 h at 130 °C resulted in the retention of the chemical structure consisting of PS-*b*-P*t*BA, and thus no deprotection occurred (Figure S2 PM-IRRAS). In addition, optical microscopy and AFM showed island and hole formation and a lack of detectable lateral nanostructure (Figures 1a and 1b), suggesting that the system adopted a surface parallel lamellar morphology, which was expected for this symmetric block copolymer. Films annealed at 150 °C for 24 h under vacuum, or in air, underwent deprotection of the P*t*BA block; the *tert*-butyl group was removed as isobutylene and formed the acrylic anhydride analogue of the polymer after loss of water (Scheme 1). The mass loss (27% theoretically) shifted the volumetric composition of the copolymer, which resulted in a change in the BCP morphology as well as in the overall film thickness. In particular, as shown in Figures 1c and 1d, the lamellar BCP transitioned to a cylindrical nanostructure, consistent with a calculated shift in PS volume fraction from 0.47 to 0.62. The morphology shift followed a similar trend to that reported by Nealey and co-workers, who noted the transformation of a cylinder forming PS-*b*-P*t*BA to a spherical morphology upon deprotection (25). As shown by the AFM

image in Figure 1d, the cylinders are oriented perpendicular to the film surface at the free interface, with small regions of parallel cylinders. However, the presence of island and hole structures, as indicated by Figure 1c, would suggest some degree of parallel orientation in the underlying film. To analyze the orientation through the thickness of the film, grazing-incidence small-angle X-ray scattering (GI-SAXS) or cross-sectional transmission electron microscopy (TEM) would be required, and this analysis is being pursued in future work. We propose that changes in the block surface energetics due to thermal deprotection and chain dynamics of the adduct explain the orientation of the BCP at the free surface. Prior to deprotection, the system exhibited a lamellar morphology where the P*t*BA block was situated at the air interface because it has a lower surface energy (31.2 mJ/m^2) compared to PS (40.7 mJ/m^2) (26). After deprotection, the system exhibited a surface perpendicular orientation as evidenced by the cylindrical morphology found using AFM. A transition in surface energetics contributed to this morphological shift as the surface energy of the deprotected PAH block (the hydrated analogue of PAH is PAA and has a surface energy in the range of 50 mJ/m^2 to 68 mJ/m^2) (36, 37) exceeds that of the PS block. The lower surface energy of PS thus favors expression of the PS block at the air interface.

The mass loss from the deprotection reaction also resulted in a measurable and visible decrease in the film thickness (see final row of Table 1). The relative film thickness change can be rationalized by calculating the change in molar volume of the BCP before and after deprotection, as expressed in eq 1

$$\frac{\Delta h}{h_0} = \frac{\Delta v}{v_0} = \frac{(v_{PS} + v_{PtBA}) - (v_{PS} + v_{PAH})}{(v_{PS} + v_{PtBA})} = 29\% \qquad (1)$$

where h is the film thickness and v is the molar volume. Using the values for v reported in Table 2, we calculated a relative thickness decrease of 29%, which agreed well with the measured film thickness change shown in Table 1. This thickness change provided a convenient way to track deprotection across a gradient library.

Annealing on a Temperature Gradient. To track the deprotection and rearrangement behavior as a function of temperature and time, films of a constant thickness (≈100 nm) were placed on a thermal gradient with a range of 185−100 °C. The thickness transition of the films was monitored in situ using a combination of the thermal IR camera and visual inspection. As noted above, the transition of films annealed on the thermal gradient was distinguished by a color change of the film propagating to lower temperatures as a function of time (Figure 2a). To map the deprotection behavior more thoroughly, and to investigate whether it was influenced by the thermal gradient itself, separate libraries were placed on different sections of the stage such that they covered different temperature ranges along the gradient. Measured positions of the front were used to track the transformation as a function of temperature and time.

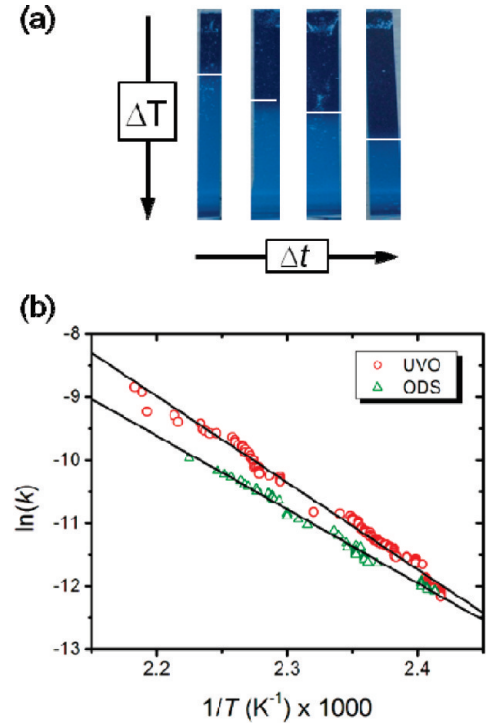

FIGURE 2. (a) Optical images of PS-*b*-P*t*BA films annealed on a thermal gradient for (from left to right) 8 h, 24 h, 30 h, and 48 h, and (b) deprotection transformation rate constants for films on UVO-treated surfaces (red circles) and ODS-modified surfaces (green triangles). The solid lines are first-order Arrhenius fits (eq 2) to the UVO and ODS kinetic data.

Figure 2b shows examples of these kinetic data, which have been fit using an Arrhenius relationship

$$k_t = Ae^{-E_a/RT} \text{ or } \ln(k_t) = \frac{-E_a}{R}\frac{1}{T} + \ln(A) \qquad (2)$$

where k_t is a transformation rate constant, A is a prefactor, E_a is the activation energy, R is the gas constant, and T is the reaction temperature. The transformation rate constants were defined as the inverse time of full deprotection at a given temperature. As Figure 2b illustrates, when plotted in this manner, the measured positions (red data points; green data points will be discussed later) of the deprotection front fall along a linear fit, regardless of the temperature range a given library covered on the gradient stage. Thus, the deprotection at a given temperature is solely influenced by the thermal conditions and unaffected by the chemical state of neighboring polymer. The Arrhenius fit yielded a calculated activation energy of $E_a = 92 \pm 4$ kJ/mol for UVO-treated substrates displaying surface hydroxyl groups. This activation energy of the transformation was in good agreement with the thermal lithography experiments of Duvigneau and co-workers, where they calculated a reaction activation energy of 93 ± 12 kJ/mol (7). Transformation rate constants for the libraries on these substrates ranged from 1.45×10^{-4} s^{-1} to 5.02×10^{-5} s^{-1}, depending on the temperature and position on the thermal gradient. The transformation rate constants also tracked with Arrhenius behavior that predicts a doubling of the reaction rate every 10 °C. The exponential

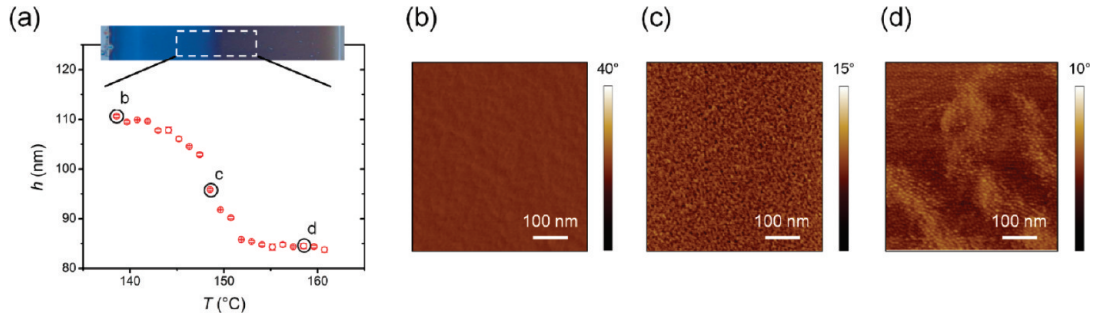

FIGURE 3. (a) Thickness measurements across the thermal deprotection front after the BCP film was annealed on the thermal gradient for 24 h. Inset is a macroscopic optical image of the film, illustrating that the deprotection front can be visually discerned. The error bars, which are smaller than the size of the symbols, indicate one standard deviation of the data, which is taken as the experimental uncertainty of the measurement. (b–d) AFM phase images at three positions along the thermal gradient corresponding to temperatures of 138, 148, and 158 °C, respectively. The AFM images suggest the formation of (b) parallel lamellae, (c) mixed morphology, and (d) perpendicular cylinders.

decay and first-order kinetics also agreed well with studies by Feng and co-workers who investigated the interfacial hydrolysis on PS-*b*-P*t*BA thin films using 3 M HCl; their study resulted in a reaction rate constant of 2.2×10^{-5} s^{-1} (11).

After 55 h of annealing on the thermal gradient, libraries were quenched to room temperature, and the film region around the deprotection front was characterized further. Thickness measurements (Figure 3a) using reflectance interferometry illustrated that the deprotection front is gradual, occurring over about 6 mm (corresponding to a temperature range of ~6 °C). AFM analysis of the same library showed the expected morphologies well below and well above the deprotection front for the respective chemical structures (i.e., PS-*b*-P*t*BA lamellae at lower temperatures and PS-*b*-PAH cylinders at high temperatures), as shown in images b and d in Figure 3. Within the transition region of the deprotection front (Figure 3c), the BCP film showed a mixed morphology between perpendicular cylinders and parallel lamellae.

The chemical changes in the block copolymer films across the deprotection front were characterized by XPS. The XPS technique, as performed, measured surface composition to a depth of approximately 10 nm (34). Therefore, any morphological transition involving mass transport into or out of the 10 nm surface region will be highlighted in our XPS measurements. High resolution spectra from the C 1s region are presented in Figure 4. These figures show spectra from native (protected) and fully deprotected regions of the block copolymer film.

The five modeled peaks are shown; the native polymer spectrum had a clear shoulder peak at 287.0 eV indicating the presence of the tertiary carbon, and a smaller shakeup peak at 291.5 eV from the aromatic resonance. The loss of the *tert*-butyl group (based on peak modeling) was measured in 1 mm increments through the deprotection front (Figure 5a). The native copolymer had the maximum *tert*-butyl content, which remained constant for the first eight 1 mm increments. The decrease in *tert*-butyl content associated with deprotection represents the release of isobutylene, the side product of the reaction. The decrease in *tert*-butyl content corresponded with a decrease in measured carbonyl content and an increase in the shakeup peak from the aromatic resonance, as shown in Figure 5b. However, the decrease in carbonyl carbon reached a plateau at a nonzero

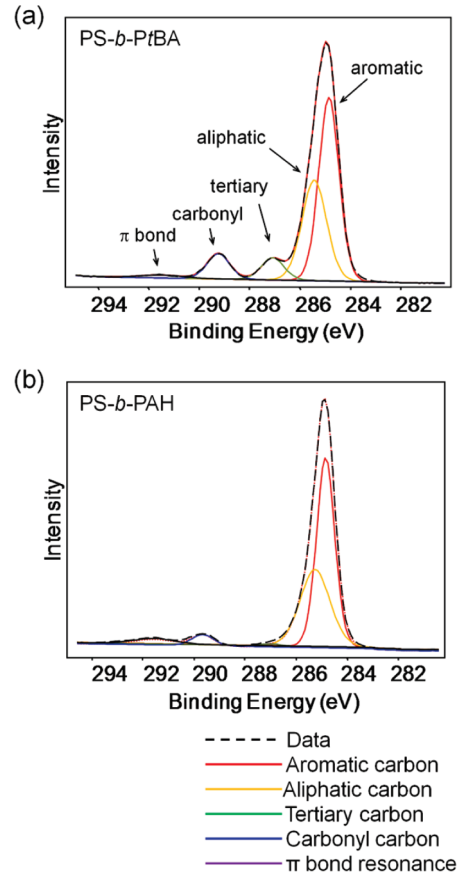

FIGURE 4. Peak fitting of high-resolution XPS C 1s spectra for (a) PS-*b*-P*t*BA and (b) PS-*b*-PAH. XPS data of (a) native film and (b) deprotected film were taken ex situ after annealing on the thermal gradient for 24 h. Note the loss of the tertiary carbon after deprotection.

value for the final measurements, whereas the *tert*-butyl content decreased to 0%. The complete loss in *tert*-butyl content was further evidence of thermal deprotection. The corresponding decrease in carbonyl carbon was attributed to a morphological transition as a result of the deprotection combined with a movement of polymer segments due to a new set of surface energy conditions. The native copolymer film was surface rich in the P*t*BA block (originally the lowest surface energy species), but as thermal deprotection proceeded, PS block (now the lowest surface energy by comparison) is preferred at the free interface, which drives the

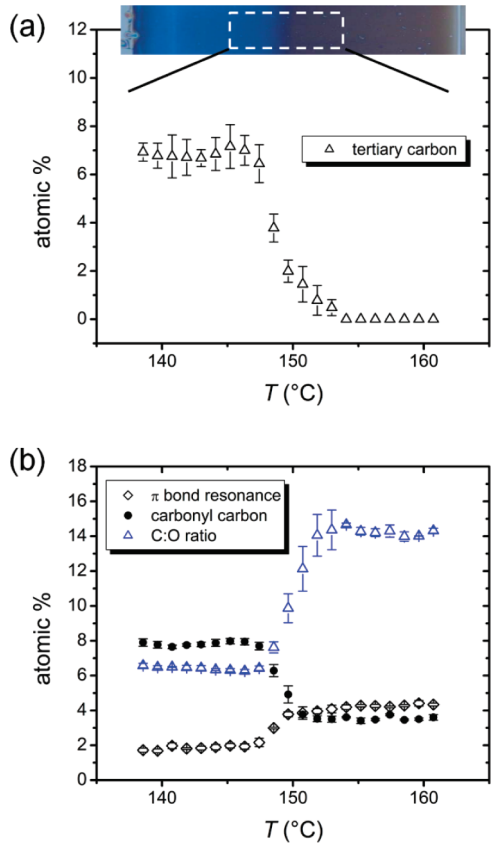

FIGURE 5. Analysis from XPS peak fitting across the thermal deprotection front after the BCP film was annealed on the thermal gradient for 24 h. (a) Atomic percent of the tertiary carbon from the P*t*BA, which exhibited a decrease as the *t*-butyl group was cleaved and removed from the film as isobutene. (b) Atomic percent of the π bond resonance (PS) and carbonyl region (P*t*BA/PAH), as well as the C:O ratio, demonstrated the concurrent thermal deprotection and morphological transition in the BCP film. The error bars indicate one standard deviation of the data, which is taken as the experimental uncertainty of the measurement. Each plotted data point consists of an average of at least four measurements at identical positions on the specimen.

formation of a wetting layer of this species. This morphological transition and surface restructuring was further supported by the dramatic increase in C:O ratio for measurements from native and deprotected BCP films (Figure 5b). The first eight positions corresponding to the native copolymer had an average C:O ratio of 7.2 as measured by XPS. This ratio increased beyond the eighth measurement eventually reaching ~14 for the final nine measurements. By comparison, the calculated C:O ratio based on the BCP stoichiometry, which is "averaged" over the entire film thickness, should decrease from 7.75 for the native film to 5.75 for the deprotected film. Accordingly, the noted increase in C:O ratio in conjunction with a total disappearance of *tert*-butyl content indicated that the morphological transition and thermal deprotection occurred concurrently, over a few nanometers near the free interface. That is, the morphology rapidly adjusted to accommodate the immediate chemistry and structure of the copolymer, rather than changing all at once when the reaction is complete. This finding suggests additional levels of complexity in controlling all aspects of the BCP behavior, but identifying conditions and causes of this behavior could be useful in fully exploiting the system for manufacturing smart devices.

Substrate Surface Effects. To examine the effects of substrate surface chemistry on deprotection, identical BCP film libraries were flow coated onto a UVO-treated surface (average water contact angle: 7.7°, see Figure 6a) and an ODS-modified substrate (average water contact angle: 83.6°, see Figure 6b). The libraries were annealed on the thermal gradient (exposed range was from 185 to 100 °C), and their deprotection fronts were monitored similarly as described above. Figure 6c shows that after 24 h, the deprotection front of the UVO-treated library progressed to lower temperatures compared to that on the ODS-modified substrate. The deprotection position of the UVO-treated library corresponded to 148 °C, which falls in line with the UVO-treated data points illustrated in Figure 2b for an annealing time of 24 h. The position of the deprotection front of the ODS-modified library corresponded to 156 °C. This difference in reaction time agreed with reports in the literature that hydroxyl groups on the surface can enhance reactivity of the deprotection reaction and illustrates how a less active substrate surface can influence this reaction (26, 27, 31). Monitoring libraries of ODS-modified substrates on the thermal gradient as a function of time allowed extraction of kinetic data from the thermal deprotection on this modified substrate just as with the UVO-treated surface. Figure 2b illustrates experimental and fitted data describing the kinetics of the thermal deprotection on an alkyl surface using eq 2 (green triangles). Fitting the data to the Arrhenius equation resulted in a calculated E_a of 88 ± 4 kJ/mol compared to 92 ± 4 kJ/mol for a hydroxyl surface. Though the lower calculated E_a for an ODS-modified surface is unexpected compared to that calculated for a hydroxyl surface, the difference of the calculated activation energies may not be statistically significant. The transformation rate constants for an ODS-modified substrate, however, reflected a magnitude slower reactivity compared to the UVO-treated surface and ranged from $k_t = 4.76 \times 10^{-5}$ s^{-1} to 5.73×10^{-6} s^{-1}, which also closely adhered to the doubling of k_t with every 10 °C. The difference between the fitted data for UVO-treated and ODS-modified substrates at all temperatures where deprotection occurs was interpreted as a difference in induction time.

Surface chemistry often plays an important role in the orientation of BCP self-assembly because it determines which block is energetically preferred to reside at the substrate (20). Indeed, when comparing UVO-treated and ODS-modified substrates, P*t*BA and PS blocks are expected to wet the substrate respectively. To examine this further, the morphology and orientation of the deprotected region were analyzed using AFM for both the UVO-treated and ODS-modified substrates. AFM phase images d and e in Figure 6 indicated that perpendicular cylinders form for both cases of substrate surface chemistry at the free interface. The similar orientations suggest that the block energetics at the air interface, rather than the substrate chemistry, dominated the domain orientation at the surface. Through-film perpendicular orientation of domains most often requires a neutral

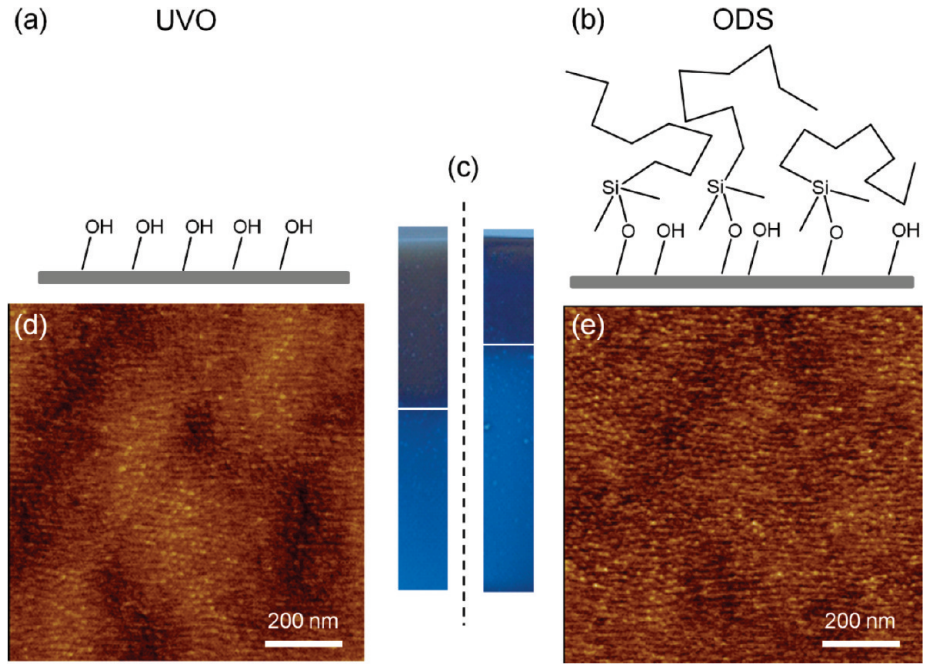

FIGURE 6. (a, b) Schematics of the surface chemistry for (a) a UVO-treated substrate, which presents primarily hydroxyl groups at the interface, and (b) a pristine ODS substrate, which presents alkyl groups at the interface. (c) Optical images of PS-*b*-P*t*BA films on the two different chemical modified substrates after annealing on a thermal gradient for 24 h. (d, e) AFM phase images of the deprotected PS-*b*-PAH on (d) UVO-treated substrate and (e) ODS-modified substrate showing perpendicular cylindrical morphologies. The *z*-scale for both AFM phase images is 10°.

substrate interface and amenable surface energetics at the air interface. Additionally, the observation of island and hole structures, indicators of nonuniform film thicknesses, are typically not found in perpendicularly oriented thin films. Accordingly, the presence of such structures in our films indicates that the thermal deprotection is likely a complex process, with multiple transformations occurring simultaneously including mass loss, morphology shift, and change in relative surface energetics, which result in a state at the free interface that exhibits locally perpendicular surface domains.

Thickness Effects. To gain insight into potential thickness effects on the deprotection reaction in thin films, we fabricated a film thickness gradient library (Figure 7a) and annealed it on an orthogonal thermal gradient. The thickness gradient spanned a range of 60 to 105 nm, and the annealing temperatures ranged from 165−100 °C. After annealing the film for 24 h (Figure 7b), the thickness gradient library was quenched to room temperature and analyzed. As shown in Figure 7c, thickness measurements orthogonal to the thickness gradient across the deprotection front on the thick and thin end (along lines 1 and 2 in Figure 7b) illustrated similar relative thickness loss due to the deprotection. At the thickest end (100 nm in thickness), the location of the deprotection front corresponded to a temperature of 145 °C, whereas at the thinnest end, the front position coincided with a temperature of 147 °C. The front positions were in good agreement with the universal plot (Figure 2b, red circles) for a 24 h anneal and within the estimated error associated with the front line. As such, the deprotection reaction appeared to be insensitive to film thickness within the measured thickness range.

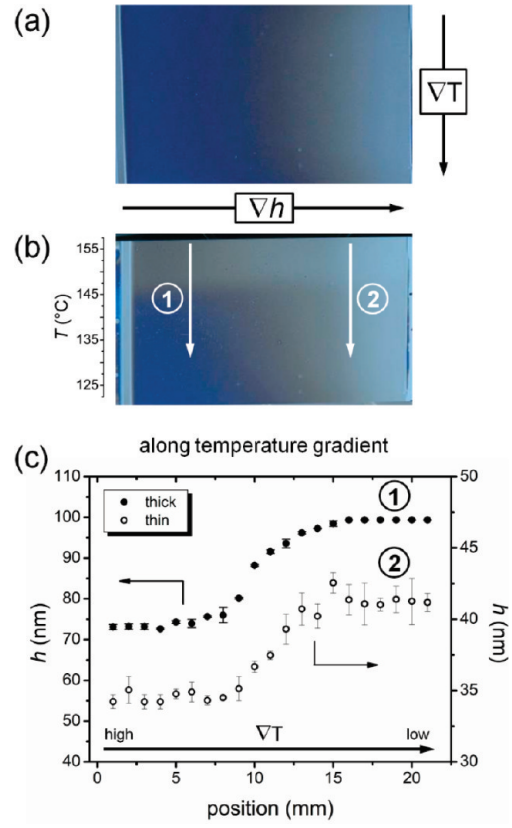

FIGURE 7. Optical images of a thickness gradient library (a) before and (b) after annealing on an orthogonal thermal gradient for 24 h. (c) Thickness measurements along the temperature gradient (across the deprotection front) for a thick film region and a thin film region. The error bars indicate one standard deviation of the data, which is taken as the experimental uncertainty of the measurement. Each plotted data point consists of an average of at least four measurements at identical locations on the specimen.

CONCLUSIONS

In this study, gradient libraries were used to examine thermally labile block copolymers in thin films. Specifically, thermal and thickness gradients were employed for the analysis of the morphology of PS-*b*-P*t*BA through its thermal deprotection reaction. The deprotection reaction resulted in a mass loss and a shift in surface energetics that transforms the BCP morphology from surface parallel lamellae to perpendicular cylinders. XPS analysis and thickness measurements were used to examine the deprotection front and to track the front motion along the temperature gradient. Arrhenius fits to the front motion data enabled the extraction of film transformation constants, which ranged from $k_t = 1.45 \times 10^{-4}\ s^{-1}$ to $5.02 \times 10^{-5}\ s^{-1}$, and an activation energy, $E_a = 92 \pm 4$ kJ/mol. The values measured using thermal gradient libraries agreed well with the results of surface hydrolysis studies in the literature. This approach to measuring transformation kinetics was also used to compare the rates of film transformation on substrates with differing chemistry. Arrhenius fits point to a significantly longer induction time for films on ODS-modified surfaces, but the film surface morphology (perpendicular cylinders) appeared insensitive to the substrate chemistry. As demonstrated using a film thickness gradient, film thickness did not seem to be an important factor in the transformation rate over the range examined. These results showed that gradients can be an effective means of examining thermally responsive BCP films and similar systems. As such, these techniques provided a way to rapidly and thoroughly map the key processing factors necessary to engineer the behavior of such materials for lithography, templating, and other nanoscale technologies.

Acknowledgment. This work was funded by NIST MSEL 70NANB9H8150 and NSF DMR CAREER - 0645586. J.Y.K. was supported by a NIST/NRC ARRA Postdoctoral Fellowship Program. J.N.L.A. was supported by a NSF Graduate Research Fellowship. J.A.H. was supported by the NIST/NRC Postdoctoral Fellowship Program. The authors thank Dr. T. Beebe, Jr., Department of Chemistry, University of Delaware, for use of his contact angle measuring system. This work is an official contribution of the National Institute of Standards and Technology.

Supporting Information Available: Figure S1 and Figure S2, which illustrate the thermal profile of the thermal gradient hot stage and PM-IRRAS results from isothermal annealing conditions (PDF). This material is available free of charge via the Internet at http://pubs.acs.org.

REFERENCES AND NOTES

(1) Amir, R. J.; Zhong, S.; Pochan, D. J.; Hawker, C. J. *J. Am. Chem. Soc.* **2009**, *131*, 13949–13951.
(2) Chang, Y.; Chen, W.-Y.; Yandi, W.; Shih, Y.-J.; Chu, W.-L.; Liu, Y.-L.; Chu, C.-W.; Ruaan, R.-C.; Higuchi, A. *Biomacromolecules* **2009**, *10*, 2092–2100.
(3) Hamley, I. W. *Nanotechnology* **2003**, *14*, R39–R54.
(4) Hamley, I. W. *Angew. Chem., Int. Ed.* **2003**, *42*, 1692–1712.
(5) Park, S.; Wang, J.-Y.; Kim, B.; Xu, J.; Russell, T. P. *ACS Nano* **2008**, *2*, 766–772.
(6) Xu, C.; Wayland, B. B.; Fryd, M.; Winey, K. I.; Composto, R. J. *Macromolecules* **2006**, *39*, 6063–6070.
(7) Duvigneau, J.; Schonherr, H.; Vancso, G. J. *Langmuir* **2008**, *24*, 10825–10832.
(8) Alexandridis, P.; Lindman, B. *Amphiphilic Block Copolymers: Self-Assembly and Applications.*, 1st ed.; Elsevier Science B. V.: Amsterdam, The Netherlands, 2000.
(9) Mistark, P. A.; Park, S.; Yalcin, S. E.; Lee, D. H.; Yavuzcetin, O.; Tuominen, M. T.; Russell, T. P.; Achermann, M. *ACS Nano* **2009**, *3*, 3987–3992.
(10) Rider, D. A.; Liu, K.; Eloi, J.-C.; Vanderark, L.; Yang, L.; Wang, J.-Y.; Grozea, D.; Lu, Z.-H.; Russell, T. P.; Manners, I. *ACS Nano* **2008**, *2*, 263–270.
(11) Feng, C. L.; Vancso, G. J.; Schonherr, H. *Langmuir* **2005**, *21*, 2356–2363.
(12) Perrin, R.; Elomaa, M.; Jannasch, P. *Macromolecules* **2009**, *42*, 5146–5154.
(13) Epps, T. H., III; DeLongchamp, D. M.; Fasolka, M. J.; Fischer, D. A.; Jablonski, E. L. *Langmuir* **2007**, *23*, 3355–3362.
(14) Fasolka, M. J.; Mayes, A. M. *Annu. Rev. Mater. Res.* **2001**, *31*, 323–355.
(15) Fasolka, M. J.; Banerjee, P.; Mayes, A. M.; Pickett, G.; Balazs, A. C. *Macromolecules* **2000**, *33*, 5702–5712.
(16) Wu, J. S.; Fasolka, M. J.; Hammond, P. T. *Macromolecules* **2000**, *33*, 1108–1110.
(17) Koberstein, J. T.; Karim, A.; Kumar, S., *Polymer Surfaces, Interfaces and Thin Films*; World Scientific Publishing: Singapore, 2000; p 115.
(18) Smith, A. P.; Douglas, J. F.; Amis, E. J.; Karim, A. *Langmuir* **2007**, *23*, 12380–12387.
(19) Sehgal, A.; Ferreiro, V.; Douglas, J. F.; Amis, E. J.; Karim, A. *Langmuir* **2002**, *18*, 7041–7048.
(20) Albert, J. N. L.; Baney, M. J.; Stafford, C. M.; Kelly, J. Y.; Epps, T. H. *ACS Nano* **2009**, *3*, 3977–3986.
(21) Albert, J. N. L.; Epps, T. H. *Mater. Today* **2010**, *13*, 24–33.
(22) Smith, A. P.; Sehgal, A.; Douglas, J. F.; Karim, A.; Amis, E. J. *Macromol. Rapid Commun.* **2003**, *24*, 131–135.
(23) Xu, C.; Fu, X.; Fryd, M.; Xu, S.; Wayland, B. B.; Winey, K. I.; Composto, R. J. *Nano Lett.* **2006**, *6*, 282–287.
(24) Park, J. H.; Sun, Y.; Goldman, Y. E.; Composto, R. J. *Macromolecules* **2009**, *42*, 1017–1023.
(25) La, Y.-H.; Stoykovich, M. P.; Park, S. M.; Nealey, P. F. *Chem. Mater.* **2007**, *19*, 4538–4544.
(26) La, Y.-H.; Edwards, E. W.; Park, S.-M.; Nealey, P. F. *Nano Lett.* **2005**, *5*, 1379–1384.
(27) Stafford, C. M.; Roskov, K. E.; Epps, T. H.; Fasolka, M. J. *Rev. Sci. Instrum.* **2006**, *77*, 023908−023908−7.
(28) Ludwigs, S.; Schmidt, K.; Stafford, C. M.; Amis, E. J.; Fasolka, M. J.; Karim, A.; Magerle, R.; Krausch, G. *Macromolecules* **2005**, *38*, 1850–1858.
(29) Meredith, C. J.; Smith, A. P.; Karim, A.; Amis, E. J. *Macromolecules* **2000**, *33*, 9747–9756.
(30) Meredith, J. C.; Karim, A.; Amis, E. J. *Macromolecules* **2000**, *33*, 5760–5762.
(31) Beers, K. L.; Douglas, J. F.; Amis, E. J.; Karim, A. *Langmuir* **2003**, *19*, 3935–3940.
(32) Genzer, J.; Bhat, R. R. *Langmuir* **2008**, *24*, 2294–2317.
(33) Buffeteau, T.; Desbat, B.; Turlet, J. M. *Appl. Spectrosc.* **1991**, *45*, 380–389.
(34) Beamson, G.; Briggs, D., *High-Resolution Spectra of Organic Polymers: The Scienta ESCA300 Database*; Wiley: New York, 1992.
(35) Brandrup, J.; Immergut, E. H.; Grulke, E. A., *Polymer Handbook*, 4th ed.; John Wiley & Sons: New York, 1999.
(36) van Krevelen, D. W. *Properties of Polymers*; Elsevier Publishing Company: Amsterdam, The Netherlands: 1976; p 86.
(37) Tsuchida, M.; Osawa, Z. *Colloid Polym. Sci.* **1994**, *272*, 184–190.

AM100695M